Design of high speed cylindrical NMR sample spinners

F. David Doty and Paul D. Ellis

Department of Chemistry, University of South Carolina, Columbia, South Carolina 29208

(Received 23 June 1981; accepted for publication 30 August 1981)

Simple approximate solutions to compressible fluid flow problems are used to arrive at useful design equations for high-speed spinning on cylindrical air bearings for NMR studies of solids. The optimum radial clearance is shown to depend on the 1/3 power of the rotor diameter, and is 0.027 mm for a 12-mm rotor, with a surface speed of one half the speed of sound, c. The required air bearing hole diameter is about 0.3 mm with a square root dependence on the rotor diameter. A few general comments are made concerning turbine design, and a simple combination impulse-reaction type is described which offers some improvement in drive efficiency. Drive air flow is shown to depend approximately on the square root of the rotor volume for a surface speed 0.5 c. Relevant data for a number of high strength materials including hard ceramics are tabulated, and limiting speeds are calculated. The design equations are verified for 8 and 12 mm rotors made from Al_2O_3 with wall thicknesses equal to 6% of the diameter.

PACS numbers: 07.58. + g, 06.60. — c

INTRODUCTION

Basically two types of high speed sample spinners have been used for NMR of solids: those after Andrew[1] employing a single conical surface for both the bearing and drive turbine, and cylindrical designs employing separate bearing and drive systems[2–5b] or a single bearing and drive surface.[5c] The Andrews rotors have the principle advantage of simplicity of construction. However, it is impossible to optimize both the drive efficiency and the stability of such a rotor. The principle disadvantage of such spinners is the difficulty of routinely obtaining stability, especially with inhomogeneous samples, at high speeds. For this reason, we have from the beginning limited our investigation to sample spinners employing separate bearing and drive systems. The first of such methods was that of Lowe,[2] which consisted of spinning on small nylon axles. However, it appears satisfactory only for solid rotors where the balance and concentricity can be maintained to within one part in ten thousand. The asymmetrical radial load produced even by a carefully packed powder will destroy such a bearing very quickly. Small, oil lubricated bearings have also been found to be unsatisfactory in that, a high flow rate of a low viscosity oil is required to prevent excessive heat build up at the bearing surface,[6] and it is difficult to conceive how a suitable oil recovery system could be adapted within the constraints of the NMR experiment.

The "obvious" solution is to use air as the lubricant since its viscosity is low, no fluid recovery system is needed, the system is clean, and variable temperature operation is feasible. However, there are drawbacks: careful design is required to avoid vibration due to the compressibility of the fluid; the extreme precision and dimensional stability required impose severe restrictions on the choice of materials; careful filtering of the air is required to avoid scoring and binding; and the design is more empirical since the flow relationships are almost impossible to solve.

Our approach, as pictured in Fig. 1, at first glance may not appear significantly different from previous cylindrical designs, except in the design of the rotor end plugs and drive jets. However, the analysis that follows will show the significance of our improvements. Rotor stability is significantly improved by making the fundamental natural resonant frequencies higher than the desired spinning frequency, and drive efficiency is improved. Sample changing is simple, and angle adjustments are generally not necessary after the initial setup.

The format of the paper is to first present an approximate isothermal analysis of the full cylindrical air bearing with pocketed orifices and arrive at recommendations for hole size, pocket size, and radial clearance. Drive power estimates are then made, and some general comments on turbine design are presented. Next we present some rotor design equations and show that the most promising choices for rotor materials are Al_2O_3, Si_3N_4, and fiber filled composites when high filling factors and high speeds are required. Finally we tabulate some design recommendations for several rotor sizes and materials.

I. AIR BEARING DESIGN

The radial load that the air bearing must support due to gravity and the impulse from the drive jets is negligibly small compared to the radial load f_r produced by asymmetrical packing of the sample. From Newton's second law we have

$$f_r = m_a \omega^2 r, \tag{1}$$

where f_r is the radial force generated by the unbalanced mass m_a at the radius r with angular velocity ω. It is conceivable that m_a may be as much as 10% of the total

 0034-6748/81/121868-08$00.60 © 1981 American Institute of Physics

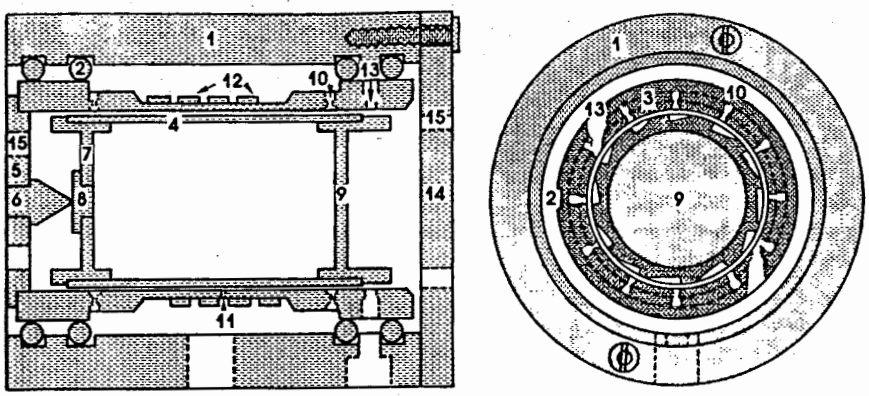

1. HOUSING	5. LOWER END PLATE	9. ROTOR DRIVE END CAP	12. NMR RECEIVER COIL
2. O-RING	6. BEARING POINT	10. AIR BEARING ORIFICE AND POCKET	13.TURBINE DRIVE JET
3. STATOR	7. LOWER ROTOR END CAP		14. UPPER END PLATE
4. ROTOR	8. BEARING BUTTON	11. COOLING AIR HOLE	15. EXHAUST HOLES

FIG. 1. Side and end section views of spinner assembly.

sample mass for samples such as granules of polymers, but it is more likely to be in the neighborhood of 1% of the total sample mass for carefully packed fine powders. A little arithmetic shows that the asymmetrical radial force produced by a one-gram sample with 1% misbalance at an average radius of 0.4 cm amounts to 1.6 $\times$ 10^6 dyn (about 3.6 lbs) at 3.2 kHz and four times that amount at 6.4 kHz. *The air bearing must either have a load capacity at least equal to the asymmetrical radial force, or else the ratio of the radial clearance to the rotor radius must be greater than the ratio of the asymmetrical mass to the total rotor mass so that the rotor can rotate freely about its center of mass.* The latter alternative requires radial clearances of at least 0.005 cm. Veeman[5a] has reported stable spinning at high speeds on air bearings with radial clearances of 0.012 cm, but our attempts to duplicate his results have not succeeded, although we have not exhaustively investigated the requirements of his design. This difficulty is due in part to the reduced bearing stiffness and hence reduced resonant frequencies that result from large clearance, low pressure bearings as we will show later. Thus, the radial clearance should be kept very small, and the air bearing should have a load capacity great enough to support the asymmetrical force required to constrain an unbalanced rotor to rotate about its geometric axis.

Referring now to Fig. 1, we see a typical cylindrical air bearing containing two circles of n equally spaced holes with several additional holes near the center. The minimum absolute manifold pressure p_i, required for a given load capacity L, in an air bearing of length l and radius r_2, with n air pockets of radius r_1 at a distance $l_1 = \pi r_2/n + r_1$ from each end with atmospheric pressure p_0 is given approximately by[6]

$$p_i > \frac{L \ln(l_1/r_1)}{l r_2} - p_0 \qquad (2)$$

when about half of the pressure drop occurs in the capillaries or orifices feeding the air pockets and the flow of air is not sonic limited. The air pockets serve mainly to keep the flow subsonic; they also tend to increase the load capacity and the stiffness of the bearing even under subsonic flow conditions.

From Eq. (2) it is clear that manifold pressures of several atmospheres will be required to support rotors of moderate misbalance at high speeds. Thus it is important to try to optimize the air bearing both for efficiency in air usage and for maximum spinning speeds. Let us begin by looking at some approximate flow equations.

In an orifice or jet the pressure drop arises primarily from the inertia of the gas. The viscosity of the gas has a negligible effect when the hole length is less than the diameter. The velocity of the jet stream (assuming irrotational flow) up to about $0.9\,c$ is given approximately by[7]

$$v \simeq \left(\frac{2(p_i - p_f)}{\gamma p_f}\right)^{1/2} c, \qquad (3)$$

where p_i and p_f are the initial and final absolute pressures, c is the speed of sound, and γ is 1.4 for diatomic gases and 1.67 for monatomic gases.The speed of sound is given by

$$c = (\gamma p/\rho)^{1/2}, \qquad (4)$$

where ρ is the density of the gas and p is the pressure. At very high pressures in properly flared jets the velocity very slowly approaches the limit of $2.24c$ for diatomic gases or $1.58c$ for monatomic gases. A useful approximation for velocities between $0.9c$ and $1.1c$ in jets is obtained by calculating the sonic limited velocity according to Eq. (3) and then subtracting $0.1c$ for each two diameters of length.

A capillary, on the other hand, has a length many times greater than its diameter and the pressure drop within the capillary arises primarily from the viscosity

of the gas. At low pressure drops with laminar flow, the average velocity is given by Poiseville's equation,

$$\bar{v} = \frac{(p_i - p_f)r^2}{8\mu l}, \tag{5}$$

where μ is the dynamic viscosity of the gas (about 0.00018 dyn s/cm^2 for air) in a capillary of radius r and length l with a pressure drop $p_i - p_f$ dyn/cm^2.

Laminar flow generally exists for Reynolds numbers below 2000. When the length is much greater than the radius, the Reynolds number for tubes is given by

$$\mathrm{Re} = 2vr\rho/\mu. \tag{6}$$

For laminar flow between stationary parallel plates a distance h apart, the average velocity is

$$v = \frac{(p_i - p_f)h^2}{12\mu l}. \tag{7}$$

The transition from laminar flow to superlaminar flow in bearings occurs when the Reynolds number for the bearing surface reaches the critical Taylor number,[8] which happens when

$$\mathrm{Re} = \omega r_2 r_c \rho/\mu = 42\left(\frac{r_2}{r_c}\right)^{1/2}, \tag{8}$$

where r_c is the radial clearance in the bearing and ω is the angular spinning frequency. At this speed the friction increases abruptly by a factor of three to four, but below this speed the frictional power loss P_f on the air bearing surface of area A and surface speed v is approximately

$$P_f = \mu v^2 A/r_c \simeq (5r_2^3 l f^2/r_c) \times 10^{-9}\ (\mathrm{W}), \tag{9}$$

where all dimensions are in centimeters and the frequency f is in Hz. This amounts typically to 5–50 W at high speeds. The air holes near the center are required to provide cooling over the central portion of the rotor, otherwise temperature rises of 25 °C could be expected at top speeds. Four holes similar to the air bearing holes but without pockets will provide sufficient air flow to keep the temperature rise below 5 °C and will facilitate variable temperature experiments.

It will soon become clear (see Eqs. (9), (16), and (28)) that the *upper practical limit* on the circumferential speed of the rotor is about 0.5 c. Hence,

$$f_{\max} \simeq 0.08c/r_2. \tag{10}$$

The optimum radial clearance is now seen from Eqs. (8) and (10) to depend only on the 1/3 power of r_2.

$$r_c \simeq \left(\frac{7000\mu^2 r_2}{c^2\rho^2}\right)^{1/3}. \tag{11}$$

This amounts to about 2.7 × 10^{-3} cm for a 12 mm rotor with air at 2 atm in the bearing. If helium gas is used, r_c may be nearly doubled thereby reducing friction, but this will seriously lower the resonant frequencies and increase the momentum loss due to leakage air as will be shown shortly.

We can now estimate the optimum bearing hole size and radial clearance for the cylindrical bearing shown in Fig. 1. Assuming an absolute manifold pressure of 3 atm, a negligible bearing hole length, and negligible inertial effects around the hole, it can be shown from Eqs. (3), (4), and (7) that when $l_1 = \pi r_2/n + r_1$ the optimum bearing hole size is given approximately by

$$r_0 \sim (2.8r_c^3/c)^{1/2} \times 10^4\ \mathrm{s}^{-1/2}. \tag{12}$$

This amounts to about 0.011 cm for a 12-mm rotor. Note that it is not explicitly dependent on n and r_2, but from Eq. (11) we see that it depends implicitly on the square root of r_2. The mass flow rate of the bearing air when the rotor is in place should be 1/3 the flow rate with the rotor removed. The above equation ignores viscous and turbulent losses in and around the orifices and assumes irrotational flow. Attempts to include these losses have suggested that the hole size be increased by 10%–30%, depending mainly on hole length, and on entrance and exit contours, and angles at the orifices.

To assure that the air flow is not sonic limited at the circumference of the air bearing orifice of radius r_0 we require pockets or recesses of the following dimensions:

$$r_1 > \tfrac{1}{2}r_0^2/r_c, \tag{13}$$

$$h > \tfrac{1}{2}r_0, \tag{14}$$

where r_1 is the pocket radius and h is the pocket depth. If the air pockets are made much smaller than this or eliminated entirely, the load capacity of the bearing will be reduced somewhat according to Eq. (2) even if the flow out of the holes is not sonic limited. If the flow here becomes sonic limited the load capacity will be seriously reduced and likewise the maximum speed of a misbalanced rotor will be reduced. If the air pockets are made much larger than required, the response time of the bearing will be reduced causing an increased tendency for instabilities at high frequencies. Moreover, the bearing hole size must be increased somewhat.

In spite of the reciprocal dependence of friction on the radial clearance, it may be desirable to use even smaller clearances than required by Eq. (11). This will result in increased bearing stiffness and hence a higher mechanical resonant frequency for the rotor. The radial stiffness ($-dF/dr$) of an air bearing is a function of the amplitude of the vibration. However, a reasonable estimate of the average static stiffness, k, of a bearing designed according to the foregoing recommendations is given by

$$k \simeq 2lr_2(p_i - p_0)/r_c. \tag{15}$$

The dynamic stiffness will be somewhat higher.[9] In some designs involving extremely small clearances the hydrodynamic stiffness may be comparable to the hydrostatic stiffness of Eq. (15). However, the Sommerfeld number[6] for the above design is typically 0.01 which implies a negligible hydrodynamic effect.

Fundamental resonant frequencies referred to as whirl

instabilities of the conical and cylindrical modes are given respectively by

$$f_1 \simeq \frac{l}{8\pi}\left(\frac{k}{I}\right)^{1/2}, \tag{16}$$

$$f_2 \simeq \frac{1}{2\pi}\left(\frac{k}{m}\right)^{1/2}, \tag{17}$$

where I is the transverse moment of inertia of the rotor about the center. It should be pointed out that the "l" in Eqs. (15) and (16) is the effective bearing length. Hence it is desirable to use a large number of bearing holes very near the ends of the rotor rather than a few holes nearer the center so as to increase l and raise the resonant frequencies—especially the conical mode. A justifiable improvement was realized in going from eight holes about $\frac{3}{8}r_2$ from each end to 12 holes about $\frac{1}{4}r_2$ from each end. Furthermore, reducing the mass of the rotor at the ends will significantly reduce the transverse moment of inertia and thereby increase f_1 to about the same as f_2. Clearly, the pressure must be made large and the radial clearance must be made small if the vibrational frequencies are to be higher than the desired spinning frequency. Since the damping term (the order of $P_f/\omega r_2$) is small compared to the driving term ($m_a\omega^2 r$, where m_a is the asymmetrical mass) for even the most carefully balanced sample, the resonance will have a high mechanical Q, and this resonant frequency is difficult to exceed.

If the mass of the stator is kept small, sufficient damping can be provided by mounting the stator on rubber O-rings so as to permit spinning above these resonant frequencies for very carefully balanced samples.[10] These resonances are more easily exceeded at low speeds. Hence, it is desirable to start spinning at nearly zero bearing pressure. The drive pressure can be slowly increased as the rotor accelerates through the resonances (which may be inaudible at low speeds) and the bearing pressure can be increased as required to prevent touchdowns.

Equations (16) and (17) are no longer strictly correct in the presence of the O-rings. The O-rings transform the spinner assembly, Fig. 1, into a system of three coupled oscillators, Fig. 2. Such a model has two important features. First, it demonstrates how the resonance frequencies of the rotor within the stator arise. Second, it provides qualitative procedures by which the resonance frequencies can be changed. For example, reducing the stator mass has two consequences—first, it lowers the effective rotor mass which appears in Eqs. (16) and (17) and further, the overall mechanical Q of the system is reduced. As a result, the resonance frequencies are increased and so is the width of these resonances.

Care must be taken in selecting the O-rings. Most O-rings are filled with about 50% carbon black for improved abrasion resistance. This may result in a high conductivity at high frequencies and thereby destroy the Q of the NMR coil. For maximum effectiveness in damping resonances, the elastomer should have a high loss

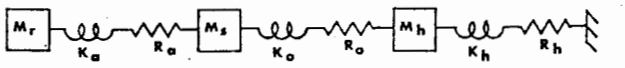

FIG. 2. A model for obtaining cylindrical mode resonant frequencies of the rotor assembly is shown. The masses of the rotor, stator, and housing are m_r, m_s, and m_h respectively; and k_a, k_0, and k_h are the stiffnesses of the air bearing, O-rings, and housing support structure. The suspension losses, R_a, R_0, and R_h, are shown explicitly as mechanical resistances (force/velocity). Typically, the rotor mass is less than half the stator mass and about one tenth the housing mass. The air bearing is about twice as stiff as the O-rings and about 10 times stiffer than the housing support. The resistances of the air bearing and of the housing support are small compared to the resistance of the O-rings.

factor, and the radial stiffness of the O-rings should be comparable to the radial stiffness of the air bearing, but a somewhat lower stiffness is required to provide isolation between the rotor vibrations and the probe. Four medium-hard Buna-N O-rings will provide a stiffness comparable to the stiffness of the air bearing with a high loss factor. Medium soft viton (a fluorocarbon) is about half as stiff with an even higher loss factor, and medium soft silicone is about one third as stiff but quite resilient. Hence, unfilled (brown) viton is probably the best choice, except for very high temperature or very low temperature applications in which silicone is superior.

Attempts to improve the NMR filling factor by winding the receiver coil on the inside central portion of the bearing are likely to be disappointing since this will significantly reduce the rotor resonant frequencies—especially the cylindrical mode. If the stator is ground from a high strength, high modulus ceramic, the wall thickness can be reduced to as little as 5% of the diameter in the central portion. The coil can be easily wound on the outside of the stator with nearly optimum filling factor and cemented in place to reduce spurious effects caused by coil vibration. The use of a low dielectric loss refractory cement may allow higher rf pulse power.

We conclude this discussion of bearing design by briefly mentioning the momentum loss due to bearing air flow. If we assume that half of the air flowing out the ends of the bearing will be accelerated to the circumferential speed v_c, it is easily shown that this represents a power loss of

$$P_m = \pi\rho r_c r_2 v_c^2 v_l, \tag{18}$$

where v_l, the longitudinal component of the velocity of the air, can be estimated from Eq. (7). This loss is typically an order of magnitude less than the frictional loss for air driven rotors and hence can usually be ignored. However, its effect can be observed by noting the slight drop in spinning speed that occurs when the bearing pressure is increased beyond that required to maintain stability.

II. TURBINES

Turbines are generally classified as being either impulse or reaction and either radial or axial.[11] Axial flow types lend themselves better to multistage design and hence can be optimized to a wide range of circumferential speeds relative to the speed of the gas. Most commercial turbines combine both impulse and reaction

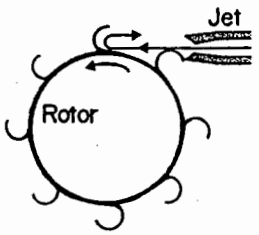

FIG. 3. Diagramatic illustration of a radial flow impulse turbine.

principles with both radial and axial flow, although axial flow generally dominates in large turbines.

An impulse turbine (Fig. 3) is driven by the impulse that results from the deflection of a jet stream. With properly contoured "buckets" the jet stream can be given a 180° deflection. When this is the case, the theoretical efficiency can approach 100% when the circumferential speed is half the speed of the jet stream. The power (in watts) then available from the jet stream of a cross-sectional area, A (cm)^2, is

$$P = \tfrac{1}{2}\rho A v^3 \times 10^{-7}\ (\mathrm{W}). \tag{19}$$

This amounts to a staggering 1.7 kW/cm^2 for air with an initial pressure of 1.7 atm and a final pressure of 1 atm. In practical MAS spinners we have observed maximum efficiencies of about 10% because of the difficulty of optimizing the turbine design.

A simple radial flow reaction turbine is shown in Fig. 4. It is driven by the reaction force that is equal and opposite to the force required to accelerate the jet stream. In this case the theoretical efficiency can approach 100% when the circumferential speed of the rotor is equal to the speed of the jet stream. The power then delivered to the rotor is the same as with the impulse turbine, Eq. (19), but the speed is doubled and the torque is halved. A more general definition of a reaction turbine would include any turbine in which the magnitude of the gas velocity increases as it passes over the rotor blades. This can be accomplished in either axial flow or radial flow by a proper choice of blade angles and sizes, such that, a substantial pressure drop occurs in the rotor rather than the stator. Most commercial turbines use a combination of impulse and reaction stages so as to more efficiently match the gas dynamics to the rotor speed. We have attempted to cut the rotor blades or flutes in such a way as to add a small amount of reaction drive for improved performance at high speeds.

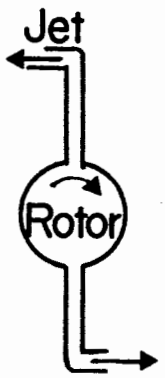

FIG. 4. Diagramatic illustration of a radial flow reaction turbine (Barker's mill).

Since typical air supply systems operate at about 4 atm, it is best to design the turbine for high pressure and low flow rates rather than low pressure and high flow rates. This allows the efficient use of a single supply for both the air bearing and the drive turbine. However, it is desirable to provide separate lines to the bearing air and drive air to facilitate spinning above the whirl instabilities. Further, variable temperature experiments are simplified since only the bearing air need be cooled or heated. This places considerably less demands on the cooling or heating system and allows high speed spinning at low temperatures without the use of helium drive gas.

For manifold pressures above 2 atm the impulse jets will be supersonic. Hence choking and shock will occur unless they are properly flared (See Fig. 5). Since this is not easily done, it is best to keep the jet throat as short as possible while keeping the angle very close to tangential. From Eqs. (9) and (11) we determine the power required to drive a rotor to $0.5c$ in air.

$$P \simeq 25 r_2^{2/3} l\ (\mathrm{W}). \tag{20}$$

Note that the power depends typically on the $\frac{5}{9}$ power (approximately square root) of the volume. From Eqs. (19) and (20) we arrive at the following total jet area (cm^2) assuming an exit velocity c and exit density ρ.

$$A \simeq \frac{5 r_2^{2/3} l \times 10^8}{\rho c^3}. \tag{21}$$

Hence, the required radius (cm) for four air jets at one end is

$$r_j \simeq 0.02 (r_2^{2/3} l)^{1/2}. \tag{22}$$

Unfortunately, experience has shown that the above result is too small by a factor of about 2. This suggests other substantial loss mechanisms such as rotor vibration and especially turbulence and rotational flow in the jets and flutes. We have tried a number of variations in flute design without observing substantial differences, although a significant advantage in efficiency is obtained by driving from one end only. The optimum flute depth appears to be about 0.9 times the jet diameter. The flutes should be cut so as to deflect the air flow backward as it leaves the end cap and thus add some reaction drive to the impulse drive.

A carefully centered hard point at the lower end (Fig. 1) maintains the axial positioning with negligible friction and wear against a Vespel SP-22 button in the center of

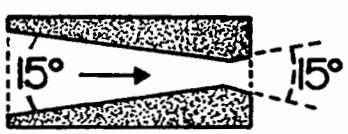

FIG. 5. Optimum jet tapers are generally around 15°. The cross-sectional area of the jet stream should increase by about 20% from the throat to the exit for a supply pressure of three atmospheres.

the end cap. (Vespel SP-22 is a graphite filled polyimide by DuPont). An end plate on the housing at the drive end *may* be required with a circle of air exit holes of appropriate size to create enough back pressure to hold the rotor against the bearing point at the opposite end.

Table I summarizes the above design recommendations for several rotor sizes. Bearing-hole size recommendations assume four short converging flow jets at one end only. The rotor resonant frequency is estimated in accordance with Eq. (16) for a rotor with very light end caps and an average density of 1.5 g/cm³ with a bearing manifold absolute pressure of 3 atm, although our experience with 12 and 8 mm versions indicates that these estimates were too high by about 20%. The extremely small size required for the bearing holes may be obtained by using watch "plate jewels." They are available from various watch makers and distributors. Microdrills are also available in these sizes.

The spinning frequency may be measured optically with a stroboscope or with an LED and phototransistor. Alternatively, a microphone and oscilloscope or spectrum analyzer may be used to measure the speed but care must be used to avoid confusion with harmonics. The piercing sound may be effectively absorbed by gluing foam rubber wedges to the interior walls of the probe thereby rendering the laboratory livable again but making it very difficult to measure the spinning frequency with a microphone.

III. MATERIAL SELECTION

This design imposes severe constraints on the choice of materials. The diametrical clearance in the air bearing is about five parts per thousand on the rotor diameter, and the cubic dependence on mass flow under laminar conditions requires that the clearance be stable within 20% or better. Thus we require an overall precision and stability of 0.1% on the diameters of the rotor and the bearing. If they can be machined to within 0.02% (that is about 0.002 mm) then we are left with 0.06% for differential thermal expansion and strain. Clearly, Table II shows that plastics—except for fiber reinforced composites—are excluded from consideration for this rotor design because of their high-thermal expansion and low Young's modulus (stiffness). Plastics have been included in the table because of their importance in other designs —particularly that of Andrews—and because of their applicability to other parts of the spinner assembly including the rotor end caps. All the plastics listed plus Macor and boron nitride are machinable with conventional metal working techniques although high-precision equipment and highly skilled personnel are required to achieve the desired precision. Al_2O_3 and the glasses are easily ground with conventional diamond tools. Si_3N_4 can be ground with *great* difficulty with special diamond tools and special equipment and techniques. (Very recent developments in the production of synthetic diamonds promise significant reductions in the price of diamond tools in the near future.) By limiting the rotor material selection to glasses and ceramics, the differential thermal

TABLE I. Design of full cylindrical air bearing with pocketed orifices.[a]

Rotor o.d. (cm)	f_{max} (kHz)	Bearing radial clearance	Bearing hole diameter	Bearing pocket diameter	Rotor resonant frequency	Jet throat diameter
0.5	11.2	0.0021	0.021	0.045	6.1	0.025
0.8	7.0	0.0024	0.025	0.060	4.5	0.037
1.2	4.7	0.0027	0.030	0.075	3.5	0.052

[a] All dimensions are cm or kHz.

expansion is easily kept to 5×10^{-6}/°C, and the strain too can be kept low enough as the following discussion shows.

From Eq. (1) it is easily shown that the centripetal pressure p_s required at the surface to constrain a fluid rotor of uniform density ρ and radius r at angular frequency ω is given by

$$p_s = \tfrac{1}{2}\rho\omega^2 r^2. \tag{25}$$

For the case of a rotor of sample density ρ_1, inner radius r_i, outer radius r_2, and wall density ρ_2 the total surface pressure is

$$p_s = \tfrac{1}{2}\omega^2[\rho_1 r_i^2 + \rho_2(r_2^2 - r_i^2)]. \tag{26}$$

The bursting pressure p_m of a thin-walled cylinder of radius r and wall thickness w is shown from elementary principles to be

$$p_m = T\,\frac{w}{r}\,, \tag{27}$$

where T is the tensile strength of the material. Thus the maximum frequency of rotation for a perfectly balanced thin walled rotor is approximately

$$f_m = \frac{1}{2\pi}\left(\frac{2Tw}{r_2(\rho_1 r_i^2 + 2\rho_2 r_2 w)}\right)^{1/2}. \tag{28}$$

Radial or circumferential resonances, or asymmetries or defects within the rotor may cause failure well below this limit—particularly in the case of glass or ceramic rotors. *A safety margin of 20% in frequency is generally adequate for plastics, but glasses and ceramics should not be operated repeatedly above 70% of* f_m. Slow crack growth in ceramics under high stress may cause them to eventually fail well below the limit calculated by the above equation.[12] Periodic annealing of Al_2O_3 rotors at 1650 °C may be necessary.

Equation (28) suggests that circumferential speeds of $0.5c$ may be reached with tough plastics such as delrin if thick walls ($w \sim \frac{1}{3}r_2$) can be tolerated, but the stretch and creep that results is unacceptable in the rotor. However, it is desirable to use a hard plastic such as vespel or delrin for the end caps so as to allow a low-pressure press fit (0.2% interference) and to facilitate removal by cooling. Adequate allowance on the end cap outer diameter (2%–4%) can be made for creep and stretch with little effect on turbine efficiency or stability. The appearance of an electrical discharge and glow around

TABLE II. Mechanical, electrical, and thermal properties of high strength insulators.

Material	Tensile[a] strength dyn/cm² × 10⁸	Young's modulus dyn/cm² × 10¹⁰	Density g/cm³	Dielectric constant 1 MHz	Dielectric power factor 1 MHz	Thermal conductivity cal/cm s ×10⁻⁴	Thermal expansion °C⁻¹ × 10⁻⁶	Micro hardness[b]
Al_2O_3 (99.8%)[c]	26	390	3.9	9	0.001	600	7	2000
BN (95%)[d]	4.5	60	2.08	4.4	0.0005	600	3	100
Diamond[e]	200	1000	3.5	5.5	0.001	18 000	2	7000
Macor[f]	8	64	2.52	5.8	0.005	40	9	250
Pyrex[g]	6	70	2.32	4.65	0.003	30	5	400
Quartz[h]	5	72	2.2	3.9	0.0001	33	0.5	500
Si_3N_4 (94%)[i]	55	320	3.23	9	0.02	200	3.5	2000
Delrin[j]	6.5	3	1.4	3.7	0.005	5.5	90	20
Epoxy[j]	7	3	1.2	3.6	0.02	4	50	20
Fiberglass[k]	25	13	1.88	4.5	0.02	4.5	30	
Kel-F[p]	2	1.3	2.1	2.45	0.01	5	60	5
Kevlar 49[n]	270	117	1.44	5	0.008	6	−2	500
Nylon[j]	7	2.5	1.2	3.3	0.01	6	100	10
Polycarbonate[j]	6	2.5	1.2	2.8	0.01	4.5	60	10
Polystyrene[j]	4	3	1.05	2.5	0.0002	2.5	70	20
Phenolic[l]	10	10	1.35	5.4	0.04	4	40	30
PMMA[j]	7	3	1.2	2.75	0.03	4.5	80	25
Polypropylene[j]	3	1.2	0.9	2.25	0.0005	5	110	5
Teflon[j]	1.2	0.4	2.2	2.1	0.0002	5.8	120	2
Vespel SP1[m]	8	2.5	1.4	3.5	0.003	8	50	25

[a] Estimates based on flexural strength data were used for Al_2O_3, macor, pyrex, and Si_3N_4. The values given for the plastics are the yield tensile strength. The rupture strength is typically 20% higher for the high modulus plastics such as Delrin and 100% higher for the low modulus plastics such as Kel-F and polypropylene. All data is at room temperature.

[b] Estimates of Knoop hardness based on various methods for comparison only.

[c] Coors Ceramics, 99.8% Al_2O_3, extruded, experimental material.

[d] Hot pressed, Union Carbide grade HBN.

[e] Glennel Corporation. Characteristics of synthetic diamonds vary widely.

[f] Corning Glass Works machinable glass–ceramic. 55% fluorinated synthetic mica, 45% borosilicate glass.

[g] Corning Glass Works. Glass fibers may have strengths as high as 10^{10} dyn/cm².

[h] Amorphous fused silica, Ref. 14.

[i] Norton Company, hot pressed NC-132, 2% amorphous magnesium silicate intergranular boundary phase, 2% tungsten. Much lower values of thermal expansion have been reported, Ref. 13.

[j] Ref. 15. See note a.

[k] NEMA Grade G-10 glass fiber reinforced epoxy. All values are orientation dependent.

[l] High quality, paper filled phenolic resin, NEMA grade X. Tensile strength ranges from 5.5 to 15 depending on quality and grain orientation.

[m] Dupont, polyimide resin.

[n] Dupont, aramid (aromatic polyamide) fibers.

[p] Ref. 16.

the end caps at high speeds is an indication that more clearance is required.

The radial strain, ϵ, the fractional increase in the radius caused by the centrifugal pressure, can be shown to be

$$\epsilon = \frac{p_s r}{Yw} = \left(\frac{f}{f_m}\right)^2 \frac{T}{Y}, \tag{29}$$

where Y is the Young's modulus of elasticity of the material. For a rotor of 1.2 cm diam made of Si_3N_4 with 0.5 mm walls that is filled with a powder of density 1.2 g/cm³, the strain amounts of 0.1% at a frequency of 5 kHz. Hence, reducing the rotor diameter by that amount should allow stable high-speed spinning without significantly affecting the stability at lower speeds although static bearing air flow will be increased significantly. However, attempts to use plastic rotors by reducing the diameter by several percent to allow for the increased stretching are not likely to be successful because of the reduced bearing stiffness at low speeds and because of the high-thermal expansion and creep of plastics.

Finally, let us consider what the optimum ratio of wall thickness to rotor radius is for maximum NMR signal sensitivity. Clearly, it lies between the limits of zero and one since the sensitivity is generally proportional to the product of the square of the inner radius and some function of the spinning frequency. The effect of the wall thickness on limiting rotor speed becomes more transparent by rewriting Eq. (28) with several dimensionless variables.

$$f_m = f'\left[1 + \beta\left(\frac{1}{2\alpha} - 1\right)\right]^{-1/2}, \tag{30}$$

where

$$f' = \left(\frac{T}{\rho_2}\right)^{1/2} \Big/ 2\pi r_2, \tag{31}$$

$$\alpha = w/r_2,$$

$$\beta = \rho_1/\rho_2,$$

When the anisotropy is comparable to, or somewhat greater than, the spinning frequency, the sensitivity increases almost in proportion to the speed. Under these conditions, one simply maximizes the product of $(1-\alpha)^2$ and f_m. The optimum thickness ratio α is seen to range from 0.12 to 0.19 as the density ratio β ranges from 0.25

TABLE III. Rotor design for sample density of 1.2 g/cm³.

o.d. (cm)	i.d. (cm)	Maximum safe speed (kHz) Al_2O_3	Maximum safe speed (kHz) Si_3N_4
0.5	0.45	7.7	11.7
0.8	0.72	4.8	7.3
1.2	1.08	3.2	4.8

to 1.0. For somewhat lower anisotropies or higher values of f', the sensitivity increases only as the square root of the frequency. Under these conditions, the optimum thickness ratio ranges from 0.08 to 0.11 as the density ratio ranges from 0.25 to 1.0. It is often desirable to operate under these latter conditions so as to obtain a spectrum with low-amplitude sidebands.

With such thin walls, the effect of sample imbalance becomes very significant, and a properly designed vibrator and rotor packing device is essential to achieve uniform particle density during the sample packing operation. The problem is more severe with smaller rotors for purely statistical reasons since the mean normalized deviation of a number of random events is proportional to the reciprocal of the square root of the number of events. A device which solves this problem is discussed elsewhere. With the aid of this device, we quickly and easily pack thin walled 8 mm rotors with all types of powder samples and spin above the resonant frequencies with no difficulty.

Table III summarizes the above considerations for several different rotor sizes and materials with sample densities of 1.2 g/cm³. The frequency calculated includes a 30% safety margin. The percent radial strain at $0.7f_m$ is 0.033% for Al_2O_3 and 0.084% for Si_3N_4. Similar calculations for empty rotors are useful for end cap design if the flutes are omitted. With flutes cut in the end cap to a depth of ⅓ the wall thickness, an additional 20% must be allowed on hard ceramics. Care must be taken to avoid concentrating the stress generated by the low modulus end cap on the end of the high modulus rotor tube, or failure will result at much lower speeds than predicted by Eq. (30). These stresses are minimized by reducing the end cap wall thickness as much as possible, and by allowing a slight radial clearance between the end cap outer diameter and the rotor tube inner diameter at the ends of the tube.

It is seen from Table III that the ratio of wall thickness to rotor diameter is constant for given circumferential speed and materials. Hence the magnetic filling factor is independent of the rotor size for a given sample and rotor material and surface speed. Assuming the electrical Q of the coil to be proportional to the ⅓ power of the volume, the NMR signal will then be approximately proportional to the ⅔ power of the volume if sufficient sample is available to fill the rotor and if the rotor can spin fast compared to the anisotropy.

ACKNOWLEDGMENTS

The authors would like to thank Dr. William H. Dawson and Dr. Ruth R. Inners for their many helpful discussions and their healthful distrust of design theory. Financial support via the National Science Foundation (CH78-18723) and the National Institutes of Health GM26295 is gratefully acknowledged. The use of the facilities at the University of South Carolina NMR Center, funded by the National Science Foundation (CH78-18723), is acknowledged, and appreciation is expressed for the use of the physics department machine shop.

The authors would like to especially acknowledge the useful discussions with members of Prof. Pine's group at Berkeley especially Dr. R. Eckman and members of Prof. Levy's group at Florida State. Their comments at the early stages of this research were helpful and have influenced the design approach summarized here.

[1] E. Andrew, L. Farnell, M. Firth, T. Gladhill, and I. Roberts, J. Magn. Reson. **1**, 27 (1969); a recent modification of this design appears to be less susceptible to rotor instabilities, V. J. Bartuska and G. E. Maciel, J. Magn. Reson. **42**, 312 (1981).
[2] I. J. Lowe, Phys. Rev. Lett. **2**, 285 (1959).
[3] E. Lippmaa, M. Alla, and T. Tuherm, *Proceedings XIX Corq. Ampere*, edited by H. Brunner, K. H. Hausser, and D. Schweitzer (Springer Verlag, Berlin, 1976), p. 113.
[4] R. Eckman, M. Alla, and A. Pines, J. Magn. Reson. **41**, 440 (1980).
[5] (a) P. A. S. van Dijk, W. Schut, J. W. M. van Os, E. M. Manger, and W. S. Veeman, J. Phys. E **13**, 1309 (1980); (b) B. Schneider D. Doskocilova, J. Babka, and A. Růzicka, J. Magn. Res. **37**, 41 (1980), and references cited within. (c) G. Baliman, M. J. S. Burgess, R. K. Harris, A. G. Oliver, K. J. Packer, B. J. Say, S. F. Tanner, R. W. Blackwell, L. W. Brown, A. Bunn, M. E. A. Cudby, and J. W. Eldrige, Chem. Phys. **46**, 469 (1980).
[6] D. F. Wilcock, *Bearing Design and Application* (McGraw–Hill, New York, 1957).
[7] A. H. Shapiro, *The Dynamics and Thermodynamics of Compressible Fluid Flow* (Ronald Press, New York, 1953), Vol. 1.
[8] *Superlaminar Flow in Bearings*, edited by D. Dowson, M. Godet, and C. M. Taylor (MEP, London, 1975).
[9] *Externally Pressurized Bearings* (Institute of Mechanical Engineers, London, 1971).
[10] J. W. Powell and M. C. Tempest, J. Lubric. Technol. **90**(4), 701 (1968).
[11] *Handbook of Fluid Dynamics*, edited by V. Streeter (McGraw–Hill, New York, 1961).
[12] *Ceramics for High Performance Applications*, edited by J. J. Burke, A. E. Gorum, and R. N. Katz (Brook Hill, Chestnut Hill, Massachusetts, 1974).
[13] *Engineering Properties of Selected Ceramic Materials*, edited by J. Lynch, C. Rudered, and W. Duckworth (American Ceramics Society, 1966).
[14] CRC Handbook of Chemistry and Physics, 57th ed., edited by R. C. Weast (CRC Press, Cleveland, Ohio, 1977).
[15] W. J. Roff and J. R. Scott, *Fibres, Films, Plastics, and Rubber* (Butterworths, London, 1971).
[16] Modern Plastics Encyclopedia **47**, edited by S. Gross (McGraw–Hill, New York, 1970).